THE STABLE STATIONARY VALUE OF THE EARTH'S GLOBAL AVERAGE ATMOSPHERIC PLANCK-WEIGHTED GREENHOUSE-GAS OPTICAL THICKNESS

by

Ferenc Miskolczi

Reprinted from

ENERGY & ENVIRONMENT

VOLUME 21 No. 4 2010

MULTI-SCIENCE PUBLISHING CO. LTD.
5 Wates Way, Brentwood, Essex CM15 9TB, United Kingdom

THE STABLE STATIONARY VALUE OF THE EARTH'S GLOBAL AVERAGE ATMOSPHERIC PLANCK-WEIGHTED GREENHOUSE-GAS OPTICAL THICKNESS

Ferenc M. Miskolczi
3 Holston Lane, Hampton VA 23664, USA

ABSTRACT
By the line-by-line method, a computer program is used to analyze Earth atmospheric radiosonde data from hundreds of weather balloon observations. In terms of a quasi-all-sky protocol, fundamental infrared atmospheric radiative flux components are calculated: at the top boundary, the outgoing long wave radiation, the surface transmitted radiation, and the upward atmospheric emittance; at the bottom boundary, the downward atmospheric emittance. The partition of the outgoing long wave radiation into upward atmospheric emittance and surface transmitted radiation components is based on the accurate computation of the true greenhouse-gas optical thickness for the radiosonde data. New relationships among the flux components have been found and are used to construct a quasi-all-sky model of the earth's atmospheric energy transfer process. In the 1948-2008 time period the global average annual mean true greenhouse-gas optical thickness is found to be time-stationary. Simulated radiative no-feedback effects of measured actual CO_2 change over the 61 years were calculated and found to be of magnitude easily detectable by the empirical data and analytical methods used. The data negate increase in CO_2 in the atmosphere as a hypothetical cause for the apparently observed global warming. A hypothesis of significant positive feedback by water vapor effect on atmospheric infrared absorption is also negated by the observed measurements. Apparently major revision of the physics underlying the greenhouse effect is needed.

INTRODUCTION

A key parameter in the study of the planetary greenhouse effect is the absorbed amount, A_A, of the surface upward infrared radiation, S_U. Greenhouse gas molecules absorb and emit the infrared radiation of the atmosphere. It has been proposed (Hansen et al. [1]; Ramanathan [2]; Bony et al. [3]) that increase of atmospheric CO_2 concentration causes persistent increase of the greenhouse effect, because proposed increase in absorption of surface upward radiation outweighs possible increase in emission of atmospheric radiation to space, with particular reference to water vapour feedback, which they say is positive.

The relevant physical quantity necessary for the computation of the accurate atmospheric absorption is the true greenhouse-gas optical thickness τ_A. The definition and the numerical computation of this quantity for a layered spherical refractive atmosphere may be found in Miskolczi [4]. Note that this quantity is conceptually different from the Planck mean optical thickness as usually defined for thin gray atmospheres; see Collins [5], Mihalas and Mihalas [6]. The fundamental difference arises from the fact that τ_A is computed from the Planck-weighted spectral hemispheric transmittance and therefore represents the true spectral feature of the infrared absorption coefficient. In short, τ_A may be expressed as:

$$\tau_A = -\ln\left[\frac{1}{\sigma t_A^4}\sum_{j=1}^{M}\pi B(\Delta\nu_j, t_A)\sum_{k=1}^{K} w^k\,\bar{T}_A(\Delta\nu_j,\mu^k)\right], \tag{1}$$

where $M = 3490$ is the total number of spectral intervals, $K = 9$ is the total number of streams, t_A is the surface temperature, B is the Planck function, σ is the Stefan-Boltzmann constant, and w^k is the hemispheric integration weight associated with the kth direction (stream). $\bar{T}_A(\Delta\nu_j,\mu^k)$ is the directional mean transmittance over a suitable short wave number interval:

$$\bar{T}_A(\Delta\nu_j,\mu^k) = \frac{1}{\Delta\nu_j}\int_{\Delta\nu_j}\exp\left[-\sum_{l=1}^{L}\sum_{i=1}^{N}\left[c^{i,l}+k_\nu^{i,l}\right]\frac{u^{i,l}}{\mu^{l,k}}\right]d\nu, \tag{2}$$

where $\mu^{l,k} = \cos(\theta^{l,k})$ and $\theta^{l,k}$ is the local zenith angle of a path segment, $c^{i,l}$ and $k_\nu^{i,l}$ are the contributions to the total monochromatic absorption coefficient from the continuum type absorptions and all absorption lines relevant to the ith absorber and lth layer respectively. $N = 11$ is the total number of major absorbing molecular species and $L = 150$ is the total number of the homogeneous atmospheric layers (shells). In eqn (2) the wavenumber integration is performed numerically by 5th order Gaussian quadrature over a wavenumber mesh structure of variable length. At least $\Delta\nu_j \approx 1$ cm^{-1} spectral resolution is required for the accurate Planck weighting. From eqn (1) follows the usual form of the transmitted and absorbed part of the surface upward radiation:

$$S_T = S_U\exp(-\tau_A), \tag{3}$$

$$A_A = S_U - S_T = S_U(1-\exp(-\tau_A)) = S_U(1-T_A) = S_U A. \tag{4}$$

In eqns (3-4) S_T is the transmitted surface upward flux, $S_U = \sigma t_A^4$ is the total surface upward flux, A_A is the absorbed part of S_U within the atmosphere, T_A is the flux transmittance of the whole air column, and $A = 1 - T_A$ is the flux absorptance. The other radiative flux components of interest are the upward and downward atmospheric emittances, E_U and E_D, subsequently, and the outgoing longwave radiation, $OLR = E_U + S_T$. Except for OLR, E_D, and S_U, the above radiative quantities cannot be directly measured. Unfortunately no computational results of E_U, S_T, A, T_A and τ_A can be found in the literature, and therefore our main purpose is to give realistic estimates of their global mean values, and investigate their dependence on the atmospheric CO_2 concentration. The accurate estimates can only be obtained by using a line-by-line radiative transfer

code and real weather balloon observations. Fig. 1. shows the definitions of the involved flux components. It is explicitly assumed that temperatures t_A and t_G are equal, the surface is black, and therefore, $S_U = S_G = \sigma t_A^4 = \sigma t_G^4$.

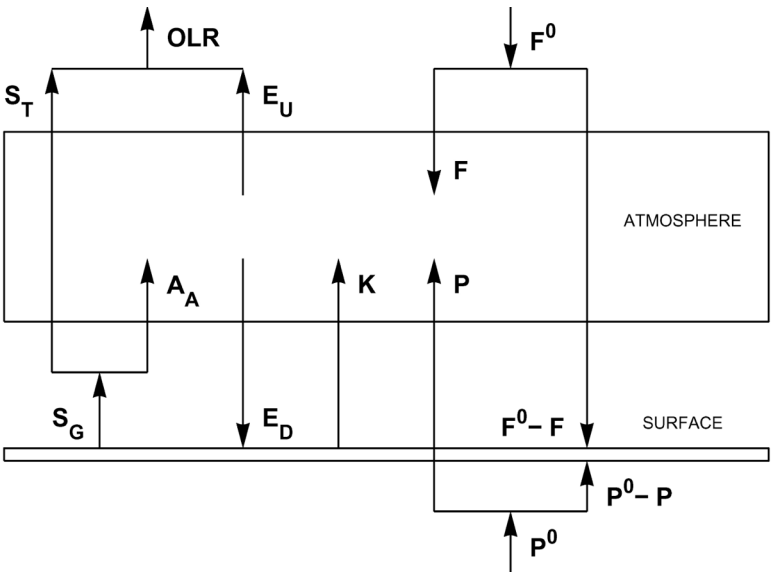

Figure 1. Semi-transparent clear sky planetary atmospheric model. F^0 is the total absorbed SW radiation in the system, F is the part of F^0 absorbed within the atmosphere, S_G is the LW upward radiation from the ground: $S_G = \sigma t_G^4$, where t_G is the ground temperature and σ is the Stefan-Boltzmann constant. The total thermal energy from the planetary interior to the surface-atmosphere system is P^0. P is the absorbed part of P^0 in the atmosphere. The net thermal energy to the atmosphere of non-radiative origin is K.

In this study the spectroscopic computations were performed by using the High-resolution Atmospheric Radiative Transfer Code, HARTCODE, Refs. 7, 8, 9, 10, 11,12. In all calculations of A, T_A, τ_A, and of the radiative flux components, the presence or absence of clouds was ignored; the calculations refer only to the greenhouse gas components of the atmosphere registered in the radiosonde data; we call this the quasi-all-sky protocol. It is assumed, however, that the atmospheric vertical thermal and water vapor structures are implicitly affected by the actual cloud cover, and that the atmosphere is at a stable steady state of cloud cover; the present quasi-all-sky protocol refers to dynamic cloud processes only by implicit assumption.

All radiative quantities mentioned hereafter, unless specifically noted to the contrary, are radiosonde data assessed in terms of the above-defined quasi-all-sky protocol. In effect, the various cloudy conditions of the actual atmosphere are regarded as maintaining their established average state, which forms a stable steady background for the present analysis.

The weather balloon observations were taken from the TIGR2 archives, Chedin and Scott [13], and from the NOAA NCEP/NCAR Reanalysis data, http://www.cdc.noaa.gov [14]. The TIGR2 dataset is used to show empirically that new relationships hold amongst certain global variables of the earth's atmospheric energy transport process. The NOAA 61-year dataset is used to demonstrate that the global average annual infrared optical thickness of the atmosphere has been unchanged for 61 years, with a value of 1.87. It will be inferred that CO_2 does not affect the Earth's climate through the greenhouse effect. In Fig. 2 the temperature and H_2O volume mixing ratio profiles of the USST76 Standard Atmosphere are compared to the global average profiles obtained from the TIGR2 and NOAA archives.

TIGR2 SIMULATIONS

1 Profile Selection Strategy

The TOVS Initial Guess Retrieval, (TIGR2), database consists of 1761 weather balloon observations. The pressure, temperature, H_2O and O_3 mixing ratio profiles are specified at 40 pressure levels between 0.05 and 1013 hPa. The soundings were collected over both hemispheres and over all seasons from 1976. For practical reasons, the number of the profiles was reduced to a reasonably small number, suitable for detailed line-by-line calculations. The TIGR2 profiles were classified according to their geographical latitudes and the seasons. Based on the latitudinal and annual distribution, 5 latitudinal belts were selected, and in each belt, one, two or three 'seasons' were established, roughly based on the solar climate. This classification of profiles resulted in 11 groups with a minimum of 57 profiles during the northern midlatitude summer, and a maximum of 332 profiles during the northern midlatitude winter. The selection of the individual TIGR2 profiles was based on the total precipitable water, u, effective H_2O temperature, T_e, and effective H_2O pressure, p_e. The final set was reduced to 228 profiles. In Table I. the characteristics of the original data set are summarized. The selected subset of the 228 profiles has a similar statistical pattern. Further details on the selection strategy and the computational parameters of the line-by-line simulations may be found in Ref. 10.

2 Analysis of the Observations with the Quasi-All-Sky Protocol

In Table 2 the ranges and the global means of some basic quantities are summarized. Global mean values were computed as the weighted average zonal means with a 5 degree latitudinal resolution. The global average TIGR2 (GAT) profile was computed similarly from the selected 228 profiles. Notice that global averaging introduces slight nonlinearity. For reference, the global average clear sky *OLR* from the ERBE Monthly Scanner Data Product is 268 Wm^{-2}, ERBE [15]. The reason of the 17 Wm^{-2} higher ERBE global average clear sky *OLR* is not yet clear. In Kiehl and Trenberth [16] the clear sky *OLR* was computed for the USST76 atmosphere and their 265 Wm^{-2} is much closer to the ERBE data. Since their water vapor column amount is much less than the global average we may speculate that the source of the discrepancy could be traced back to the anisotropy corrections of the ERBE measurements.

The data are here described in terms of three relationships between various empirically measured quantities. The three relationships are referred to here as (1) radiative exchange

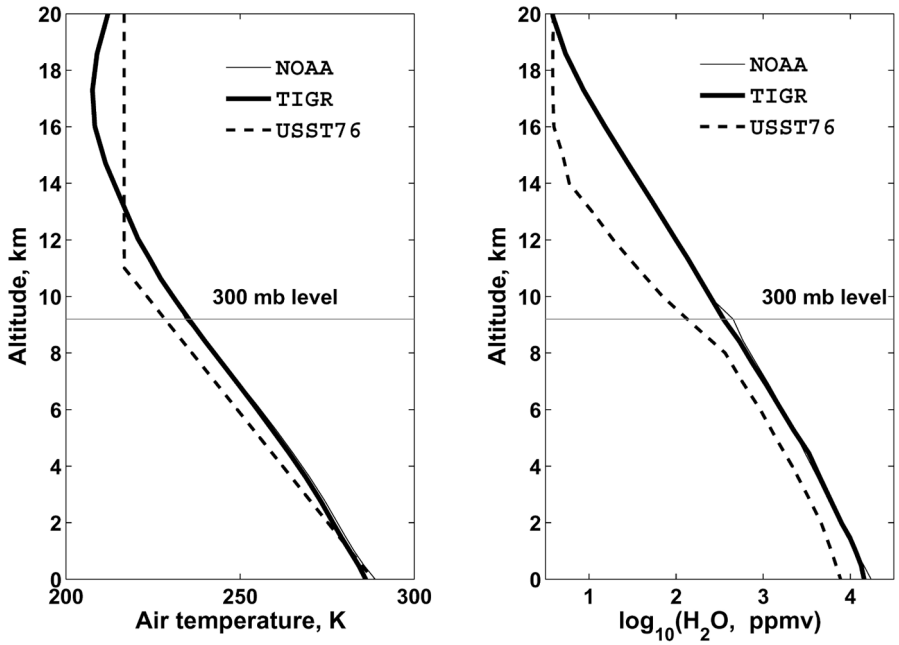

Figure 2. Temperature and H_2O profile comparisons. The NOAA and TIGR2 global average profiles are in good agreement, while the USST76 atmosphere significantly differs both in thermal structure and water vapor column amount. The NOAA and TIGR2 H_2O column amount is 2.6 precipitable cm (prcm) while the USST76 atmosphere contains only about half of this amount. Since H_2O is the most important greenhouse gas, apparently the USST-76 Atmosphere is not suitable for global radiative balance studies.

equilibrium between land-sea surface and atmosphere, (2) quasi-radiative transfer coefficient from land-sea emittance to *OLR*, and (3) global average atmospheric up-down emittance ratio.

Because the radiative exchange equilibrium and the quasi-radiative transfer coefficient relationships fit the individual radiosonde ascents from the wide variety of sampled climate conditions, they cannot in principle provide explicit direct information about the global average energy transfer, which is the object of interest for this work. The third relationship, the global average up-down emittance ratio, on the other hand, has no explicit information about single radiosonde ascents, but does complete a simple model of the global average energy transport process, which we here call the quasi-all-sky model.

RELATIONSHIPS AMONG THE RADIATIVE FLUXES IN THE QUASI-ALL-SKY MODEL

1 Radiative Exchange Equilibrium Between Land-Sea Surface and Atmosphere

One of the first and most interesting discoveries was the relationship between the absorbed surface radiation and the downward atmospheric emittance. According to

Table 1. Average characteristics of the TIGR2 subset containing 1761 profiles in 11 classes. M is the number of profiles, u is the H_2O column amount in prcm, T_e is in K and p_e is in hPa.

Class	Region and season	M	u	T_e	p_e
1	Arctic - summer	112	1.0	263	795
2	Arctic - winter	295	0.3	250	779
3	North - midlat. - summer	57	2.7	281	797
4	North - midlat. - fall /spring	88	1.1	266	804
5	North - midlat. - winter	332	0.9	263	804
6	North/South - tropical	114	3.6	285	816
7	South - midlat. - summer	131	1.6	271	808
8	South - midlat. - fall/spring	155	1.0	264	805
9	South - midlat. - winter	151	1.1	269	823
10	Antarctic - summer	157	0.5	255	783
11	Antarctic - winter	169	0.3	250	774

Ref. 4, for each radiosonde ascent the

$$E_D = A_A = S_U - S_T = S_U(1-\exp(-\tau_A)) = S_U(1-T_A) = S_U A \tag{5}$$

relationships are closely satisfied. The concept of radiative exchange was the discovery of Prevost [17]. It will be convenient here to define the term *radiative exchange equilibrium* between two specified regions of space (or bodies) as meaning that for the two regions (or bodies) A and B, the rate of flow of radiation emitted by A and absorbed by B is equal to the rate of flow the other way, regardless of other forms of transport that may be occurring.

Table 2. Ranges and the global averages of the different physical quantities. Fluxes are in Wm^{-2}, u is in prcm, t_A is in K.

Quantity	Minimum	Maximum	Global Average	GAT
t_A	**232.25**	**309.62**	**285.34**	**286.04**
S_U	**164.98**	**521.10**	**381.88**	**379.64**
u	**0.0507**	**6.836**	**2.533**	**2.637**
E_U	**83.74**	**256.71**	**188.94**	**192.7**
E_D	**103.35**	**429.69**	**308.70**	**310.49**
T_A	**0.0497150**	**0.391204**	**0.173344**	**0.15422**
$S_T = S_U T_A$	**22.246**	**111.92**	**61.094**	**58.54**
$OLR = E_U + S_T$	**150.64**	**297.62**	**250.05**	**251.25**
$\tau_A = -\ln(T_A)$	**0.9385**	**3.0014**	**1.8736**	**1.8693**

In Miskolczi [4] the relationships in eqn (5) were ascribed to Kirchhoff, but as noted above, radiative exchange equilibrium was first understood and described in 1791 by Ref. 17. Here we shall refer to the equality $E_D = S_U A$ as radiative exchange equilibrium between land-sea surface and atmosphere. Apparent violations of this law are due to

the anisotropy in the E_D radiation field, and may be corrected by an empirical hemispheric emissivity factor. From the TIGR2 data the global average hemispheric emissivity is $\overline{\varepsilon} = 0.967$. The mechanism of the equality $A_A = E_D$ is shown in Fig.3. Here the contribution density functions are plotted for the E_D and A_A fluxes. The two plots show that up to about 2 km altitude the source density of E_D and the destination density of A_A match precisely at each altitude.

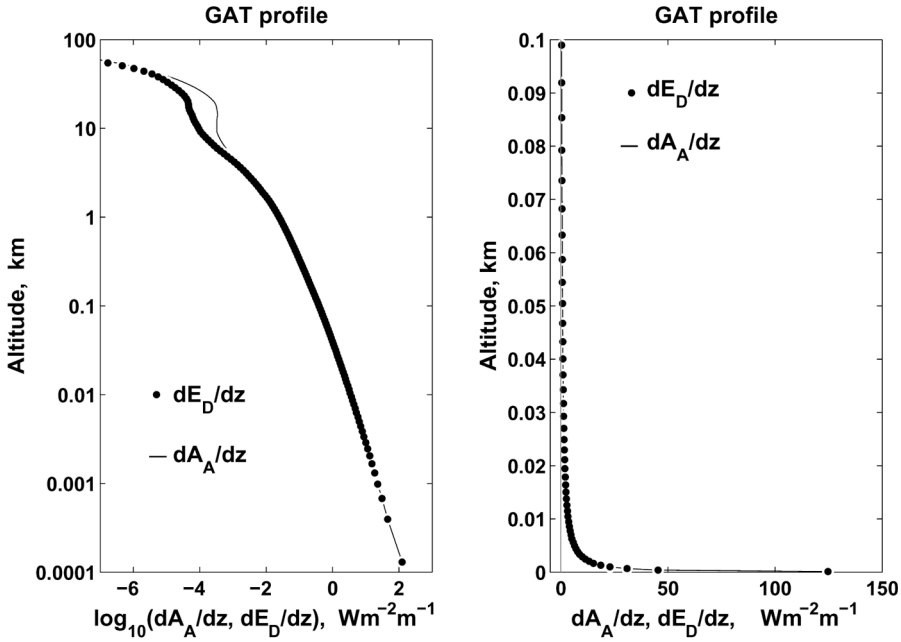

Figure 3. The law of radiative exchange equilibrium. The $E_D = S_U A$ relationship holds because the contribution of a layer to the downward emittance is equal to the absorbed surface upward radiation in the same layer. This law turned out to be valid for any cloud layer in the atmosphere and even holds true in the cloud free Martian atmosphere (see Fig. 4).

From eqn (5) follows the

$$\tau_A = -\ln(1 - E_D/S_U) \tag{6}$$

relationship which gives an independent estimate of τ_A through the surface-based observations of the E_D and S_U fluxes. Using the numerical data in Table 2 and $\overline{\varepsilon}$, the global average optical thickness for the GAT profile is $\tau_A = -\ln(1 - E_D/(\overline{\varepsilon}\, S_U)) = 1.869$. This is in good agreement with the direct computation using the $\tau_A = -\ln(T_A)$ definition. We may look in another way at the radiative equilibrium between the land-sea surface and the atmosphere. We imagine that the surface that upwardly emits A_A, and the upward facing detector surface for E_D, are lifted to various altitudes. The simulations are plotted in Fig. 4, and we see that the virtual A_A and E_D at all altitudes are equal.

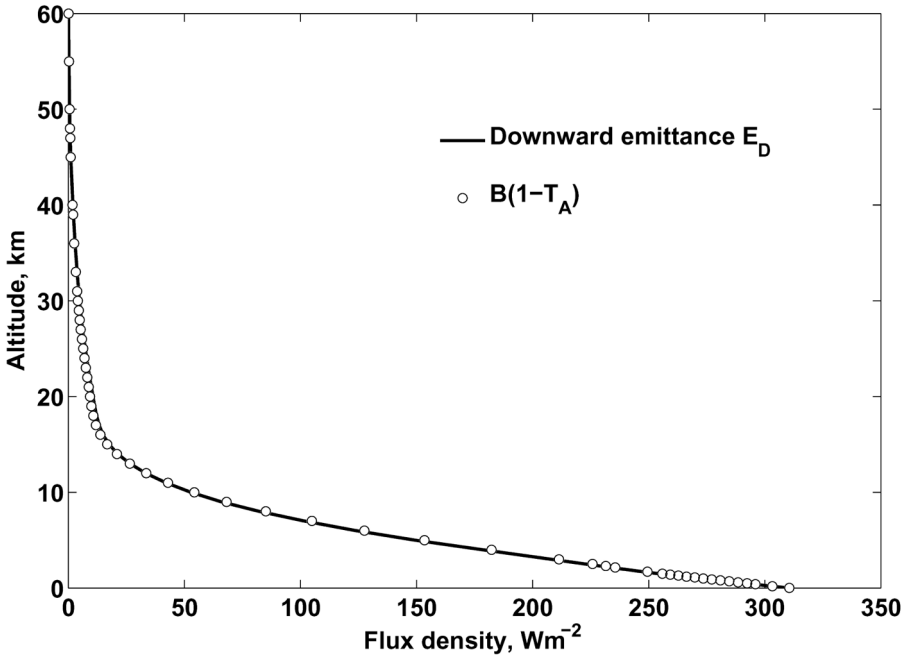

Figure 4. Radiative exchange equilibrium at altitudes above the surface. The plot shows that, independently of the altitude z, $A_A(z)$ from an upward emitting surface at z and E_D (z) from the atmosphere above are equal. Here we used the GAT atmosphere, $A_A(z) = B(z)(1 - T_A(z))$, $B(z) = \overline{\varepsilon}\,\sigma\, t_A^4(z)$, and $t_A(z)$ is the temperature profile. $E_D(z)$ may be measured by an up-looking detector at altitude z.

Another aspect of the radiative exchange equilibrium between land-sea surface and atmosphere is their spectral contents. For a hypothetical atmosphere in isothermal equilibrium with the surface $(S_U \equiv B(\mathrm{z}) \equiv \bar{B}$ and $S_U^\nu = B^\nu(\mathrm{z}) = B^\nu)$ the spectra of atmospheric and surface radiations would match exactly. Then, with the monochromatic A_A^ν, E_D^ν, S_U^ν, τ^ν, T^ν and B^ν obeying the Beer law, we may write:

$$A_A - E_D = \int_0^\infty [A_A^\nu - E_D^\nu]\, d\nu = \int_0^\infty [S_U^\nu (1 - e^{-\tau_A^\nu}) - \int_{T_A^\nu}^1 B^\nu\, dT^\nu]\, d\nu = 0. \qquad (7)$$

Fig. 5 shows the spectral A_A^ν and E_D^ν for four example radiosonde ascents. The spectral $A_A^\nu - E_D^\nu$ differences (shaded areas) in the relatively transparent spectral regions are related to the differences in the close-to-surface thermal structure of the atmosphere.

In the Antarctic summer case $A_A - E_D = 15.8$ Wm^{-2}, (5.2 % of S_U). In the Antarctic winter A case $A_A - E_D = -9.3$ Wm^{-2}, (–5.5 % of S_U). Here the strong temperature inversion resulted in the rare situation where $A_A < E_D$. These two cases are the observed maximum violations of the radiative exchange equilibrium law. In many cases the spectral differences compensate each other resulting in negligible differences

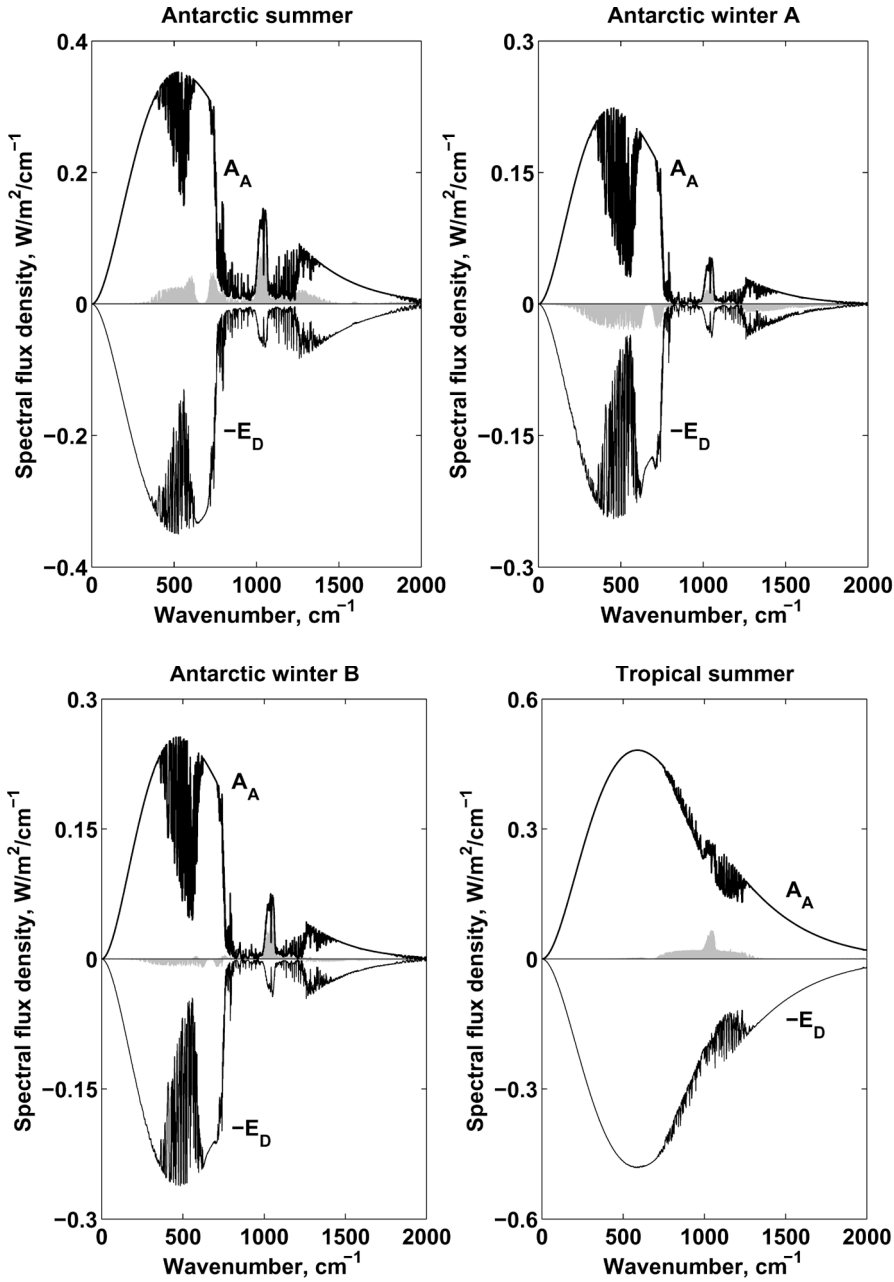

Figure 5. Violation of the radiative exchange equilibrium law. In each plot the negative spectral E_D^{ν} is plotted for clarity. The gray shaded area indicates $A_A - E_D$. The global average bias is about 3 % of S_U.

in $A_A - E_D$. For example, in the Antarctic winter B case $A_A = E_D$. As a general rule, the warm and humid atmosphere follows the radiative exchange equilibrium law better. In the Tropical summer case the bias is 11.1 Wm^{-2}, 2.5 % of S_U.

The zero dimensional energy balance model presented in Fig. 1 shows that the radiative exchange equilibrium requires the $S_U - (F^0 + P^0) = E_D - E_U$ and $E_U = P + K + F$ relationships among the fluxes. Total radiation to space from the bulk of the atmosphere is here called E_U. The source contribution profile of E_U is shown as d$Eu(z)$/dz in Fig. 6. This shows a local removal of local internal energy from the body of the atmosphere by radiation to space. Maintaining local thermodynamic equilibrium, and the steady state of the local internal energy, energy is locally dissipatively supplied by P and K and F for such radiation. Since $E_D = A_A$, on average the atmosphere does not cool radiatively to the land-sea surface, and the land-sea surface does not warm radiatively from the atmosphere. In this model, radiative surface cooling occurs only to space, by the S_T flux term. On average, atmospheric heating and cooling of the land-sea surface occurs only by non-radiative transfer.

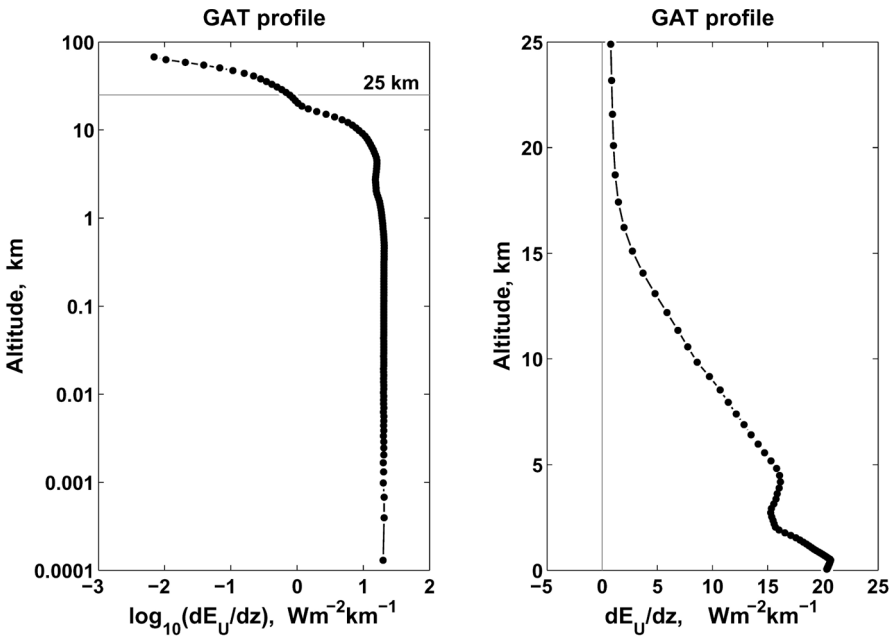

Figure 6. Contribution density function to the upward emittance. The significant part of E_U comes from the lower 25 km altitude range. About half of E_U comes from below 6 km. The dots indicate the levels where dE_U / dz was computed.

2 Quasi-Radiative Equilibrium Model

Let us consider the earth's atmospheric energy transport process in a heuristic one-dimensional abstraction in which radiative and material transport are abstracted into a single total energy transport. Now let us model that abstraction by a quasi-radiative

equilibrium. This model has been detailed in Ref. 4. In brief, it supposes that solar energy is absorbed at the land-sea surface, and from there it is radiated to space through and by a finite partially transparent atmosphere. The quasi-radiative model is expressed as a relationship between important overall energy transport variables. $S_A = \pi B(\hat{\tau}_A)$ is the source function at the bottom of the atmosphere; S_G is the upward emitted flux from the land-sea surface; τ_A is the model quasi-radiative flux optical thickness of the atmosphere: and, *OLR* is the total outgoing longwave (infrared) radiation. The quasi-radiative equilibrium defines a quasi-radiative transfer coefficient: $f(\hat{\tau}_A) = 2/\left(1 + \hat{\tau}_A + \exp(-\hat{\tau}_A)\right)$. The relationship is

$$OLR = (S_A A + S_G T_A) f(\hat{\tau}_A). \tag{8}$$

In the case in which the land-sea surface and the atmosphere in contact with it are at the same temperature, then we may think of a common upward flux S_U and set the land-sea surface emissivity to unity, so that we have $S_U = S_G = S_A$ and eqn (8) takes the following simple form:

$$OLR / S_U = f(\hat{\tau}_A). \tag{9}$$

The relationship of eqn (9) gives a fair but not perfect fit to the individual radiosonde ascents and a very good fit for the global average, see Fig. 7. The measured optical thicknesses, τ_A, in the Earth's atmosphere lie mostly in the range $1 < \tau_A < 3$. That the three global average optical thicknesses lie close to $\tau_A \cong 1.87$ is an indication that the global average atmosphere has a preference in setting its infrared optical properties.

While the fit to the individual radiosonde ascents is far from exact, the main interest of the quasi-radiative equilibrium model is in what it says about the global averages of the components of energy transfer. That it fits the data, and has a simple rationale and no arbitrary constants, is enough recommendation for the present purposes.

3 Global Average Atmospheric Up-Down Emittance Ratio

Further investigation of the meridional distribution of the fluxes revealed another simple relationship between the global average $\overline{E}_D$ and $\overline{E}_U$ (in the following equations the 'bar' over the variables denotes the spatial averaging over the globe):

$$\overline{E}_D / \overline{E}_U = 5/3. \tag{10}$$

This relationship was empirically validated for the GAT profile and by the averages of the individual TIGR2 simulations, see Fig. 8. From eqn (5) and eqn (10) we obtain the $\overline{OLR} / \overline{S}_U$ flux density ratio as:

$$\overline{OLR} / \overline{S}_U = \frac{3 + 2\overline{T}_A}{5}. \tag{11}$$

We note, that based on the empirical $\overline{S}_U = 2\overline{E}_U$ and $\overline{S}_U = 3\overline{OLR}/2$ relationships and some theoretical considerations eqns (10–11) were already predicted in Ref. 4.

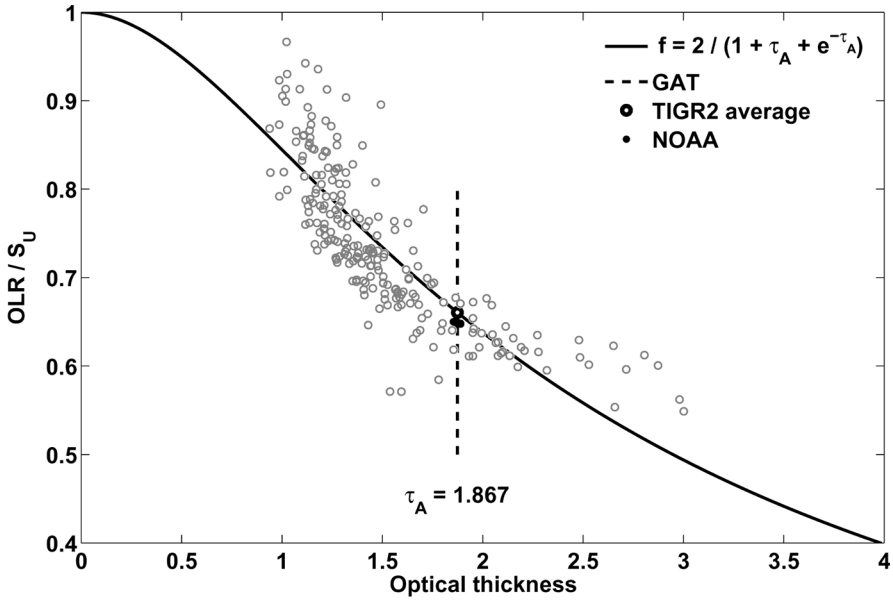

Figure 7. The gray open circles are the 228 TIGR2 ascent data, and the 61 black dots, not visibly resolved in this diagram because they are so nearly coincident, are the NOAA annual averages. The black open circle is the average of the 228 ascent data and dashed line is the GAT optical thickness.

4 Quasi-All-Sky Model of the Earth's Global Average Atmospheric Energy Transport Process

We can now consider an atmosphere which follows the three relationships, namely radiative exchange equilibrium between land-sea surface and atmosphere, the quasi-radiative transfer coefficient, and the global average atmospheric up-down emittance ratio. As noted above, these relationships are found by analysis of the empirical observations with the quasi-all-sky protocol, and the model they provide is called here the quasi-all-sky model. The three relationships mathematically imply an equation for the global average true greenhouse-gas optical thickness of our quasi-all-sky atmospheric model. Eqn (9) and eqn (11) combine to make an equation that can be solved numerically for τ_A:

$$\frac{3+2\exp(-\tau_A)}{5} = \frac{2}{1+\tau_A+\exp(-\tau_A)}. \tag{12}$$

The solution of eqn (12) is τ_A = 1.86756, in good agreement with the observed TIGR2 and NOAA averages and the GAT results presented in Fig. 7.

The three relationships of the quasi-all-sky model provide a logical structure in terms of which we can consider the possible stability of the Earth's greenhouse effect. This model is characteristic of the Earth's atmosphere. A different model is needed for Mars, where eqn (10) is replaced by the relation $\overline{E}_D / \overline{E}_U = 3/2$. For the Earth, eqn

(12) suggests that as long as the $3\overline{E}_D = 5\overline{E}_U$ and $\overline{OLR} = \overline{S}_U \overline{f}$ conditions hold there may not be any change in the surface greenhouse temperature. According to the IPCC's standpoint the anthropogenic global warming (AGW) is due to increased CO_2 emission, therefore, the possible empirical constancy of the annual global average τ_A in the Earth's atmosphere, or its variation around the $\tau_A = 1.86756$ theoretical value, is of particular interest. In the next section this question will be discussed.

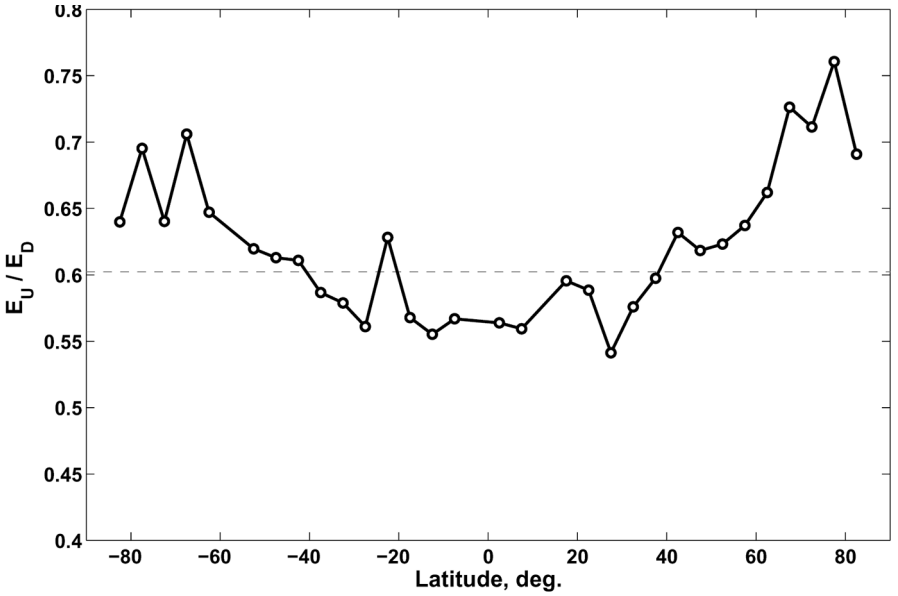

Figure 8. Meridional distribution of the E_U / E_D flux density ratio. The thin horizontal line is the global average. Open circles are averages for latitudinal belts of 5 degree width. The $\overline{E}_U / \overline{E}_D \cong 3/5$ global relationship is evident.

NOAA SIMULATIONS

1 IPCC View of Climate Sensitivity to Greenhouse Gas Increase

The IPCC has been using a special formalism for discussion of the long term response of the climate system to greenhouse gas perturbations. Their formalism states a virtual no-feedback effect of CO_2 on land-sea surface temperature, and thence states an after-feedback predicted eventual effect on that temperature. The sequence of the IPCC calculations is (1) spectroscopic simulation of the primary virtual no-feedback effect of CO_2 doubling, as it increases the greenhouse-gas optical thickness of the atmosphere, not allowing for any response of the atmosphere at this stage of the procedure; (2) estimation of how much this primary virtual no-feedback effect leads to a primary virtual increase in the surface temperature; (3) based on the entire long-term dynamics of the system, all the diverse feedback effects from the surface temperature change are then calculated, so as to yield a calculated eventual after-feedback effect. The difference between the primary virtual increase (2) in the surface temperature and the calculated eventual after-feedback effect (3) is formally regarded as a virtual feedback effect.

The main argument of the IPCC is stated in terms of this formalism: it is that there is strong positive feedback by water vapor effect on the greenhouse-gas optical thickness.

This IPCC formalism is not used in the present article, because it is considered here that taking the calculations through the primary no-feedback virtual surface temperature increase is far too indirect and complicated and fraught with un-assessable risk of error, and is utterly superfluous and apparently physically misleading. Here the eventual after-feedback effect of CO_2 on the greenhouse-gas optical thickness is assessed directly without intervening virtual surface temperature calculations.

2 Input Radiosonde Observations

About a year ago Ken Gregory suggested to test the constancy of the global average τ_A using the NOAA Earth System Research Laboratory (Ref. 14) time series data archive, and he kindly supplied me with the atmospheric profile information for the 1948–2008 (61 years) time period. In Fig. 9 the observed temperature, H_2O and CO_2 trends are presented.

A quick look at the data immediately shows that the range of the variations in the annual mean over the 61 years are very small: 58.87 atm-cm_{STP} in CO_2, –0.0169 prcm in H_2O, and 0.687 K in surface temperature. The related year-to-year changes are also very small, 0.35 %/year in c, 0.0106 %/year in u, and 0.0039 %/year in t_A. Obviously, there is strict and high requirement on the sensitivity and numerical accuracy of the computed fluxes and flux optical thicknesses.

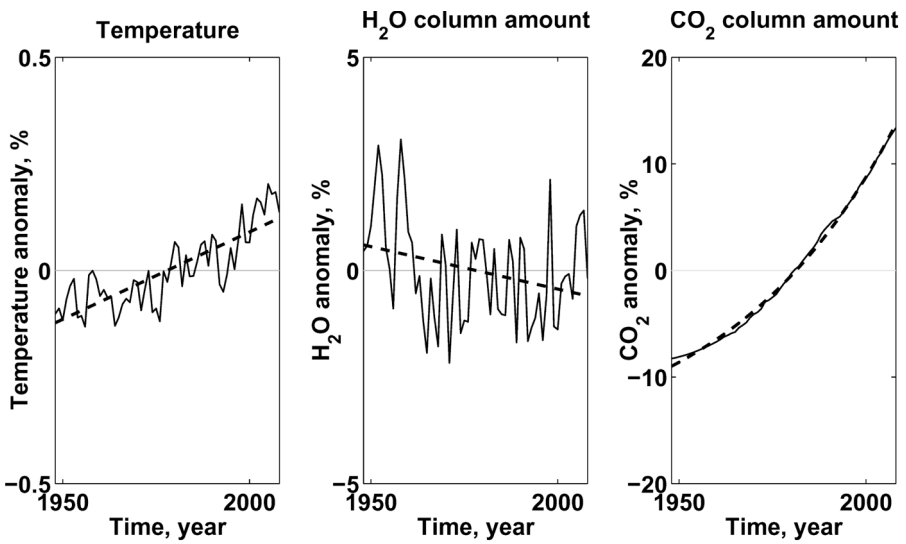

Figure 9. Temperature, t_A, H_2O, u, and CO_2, c, trends in the annual global mean reanalysis time series. The reference u, c, and t_A, are 2.61 prcm, 272.1 atm-cm_{STP}, and 288.9 K. The thin solid lines are the annual mean values. We should note, that recently there is an unsettled debate about the accuracy of the early upper tropospheric water vapor observations, see for example Paltridge at al. [18].

The NOAA time series optical depth computations were based on a slightly modified version of HARTCODE, i.e. it was set up to meet with the above mentioned

strict requirements of the computational accuracy. A short sensitivity summary is presented in Table 3. At these sensitivity runs the 61 year NOAA average atmospheric profile, (NAV) was used. Regarding the relative importance of the CO_2 and H_2O it was found that 1 ppmv increase in CO_2 concentration (equivalent with 0.8 atm-cm_{STP} increase in column amount) can be compensated by 0.3 atm-cm_{STP} (2.4×10^{-4} prcm column amount) decrease in H_2O. In other words, CO_2 doubling would virtually, with no feedback, increase the optical thickness by 0.0246. Calculations here show that an equivalent amount of increase can be caused by 2.77 per cent increase in H_2O. There is also a direct no-feedback effect of temperature on the greenhouse-gas optical thickness and calculations here show that a virtual no-feedback equivalent increase could alternatively be caused by 2.65 K decrease in the temperature at each atmospheric level. As we mentioned earlier such virtual sensitivity tests are made without dynamic feedback changes in other atmospheric profile variables. According to Table 3 HARTCODE adequately responds to the extremely small changes of the most important input parameters.

Table 3. HARTCODE sensitivity tests using the NAV profile. Fluxes are in Wm^{-2}, Δu is in prcm, Δc is in atm-cm_{STP} Δt_A is in K. The transmittance ΔT_A is dimensionless, ΔE_D, ΔOLR, ΔS_T, ΔE_U, and ΔS_U are in Wm^{-2}. The reference u, c, and t_A, are 2.61 prcm, 272.1 atm-cm_{STP}, and 288.9 K. All numerical data are multiplied by10^4.

Δu	Δc	Δt_A	ΔE_D	ΔOLR	ΔS_T	ΔE_U	ΔS_U	ΔT_A
0	0	1	3.9	3.7	1.4	2.4	5.4	1.4E-3
0	0	−1	−3.9	−3.8	−1.3	−2.4	−5.3	−1.4E-3
2.6	0	0	56.4	−19.5	−52.8	33.4	0	−1.4E-1
−2.6	0	0	−56.5	19.4	52.9	−33.4	0	1.4E-1
0	272	0	2.2	−3.7	−1.9	−1.7	0	−4.9E-3
0	−272	0	−2.2	3.6	1.9	1.8	0	4.9E-3

While the dependence of the optical thickness on the absorber amount originates from the spectral or monochromatic Beer law, it is not feasible to express this by a summary explicit analytical function. The reason is the spectral overlapping of the absorption bands of the individual absorbers. The dependence of the optical depth on the temperature is also extremely complex and again cannot feasibly be described by an explicit analytical expression. The above dependences can only be diagnosed by using the LBL method for the transmittance computation in conjunction with a realistic properly stratified spherical refractive real (or model) atmosphere which is subjected to temperature and absorber amount perturbations.

3 Investigation of the Proposed Constancy of the Global Average Value of τ_A

To investigate the proposed constancy with time of the true greenhouse gas optical thickness, we now simply compute τ_A every year and check the annual variation for possible trends. In Fig. 10 we present the variation in the optical thickness and in the atmospheric flux absorption coefficient in the last 61 years.

According to Fig. 10 the trend in τ_A is 1.5×10^{-3} % year^{-1} and the total absolute change in the 61 years is $\Delta\tau_A = 0.0018$. The trend in A is 5.4×10^{-4} % year^{-1} and the total absolute change in the 61 years is $\Delta A = 0.00028$.

Here we have to make a fine point. In a hydrostatic atmosphere, given a constant pressure range, the top altitude is a function of the profile of the virtual temperature. However, the layer absorber amount is proportional to the layer thickness, therefore the observed warming trend of the atmosphere may introduce an unwanted effect in the optical thickness trend through the technical computation of the absorber amount. The correlation between τ_A and the top altitude is rather weak. Correcting our results for the above effect by subtracting the trend in the top altitude (7.6750×10^{-4} km/year) the final trend and the absolute change are reduced to $\Delta\tau_A / \Delta t = 8.08\times10^{-4}$ %/year and $\Delta\tau_A = 0.0009213$, respectively.

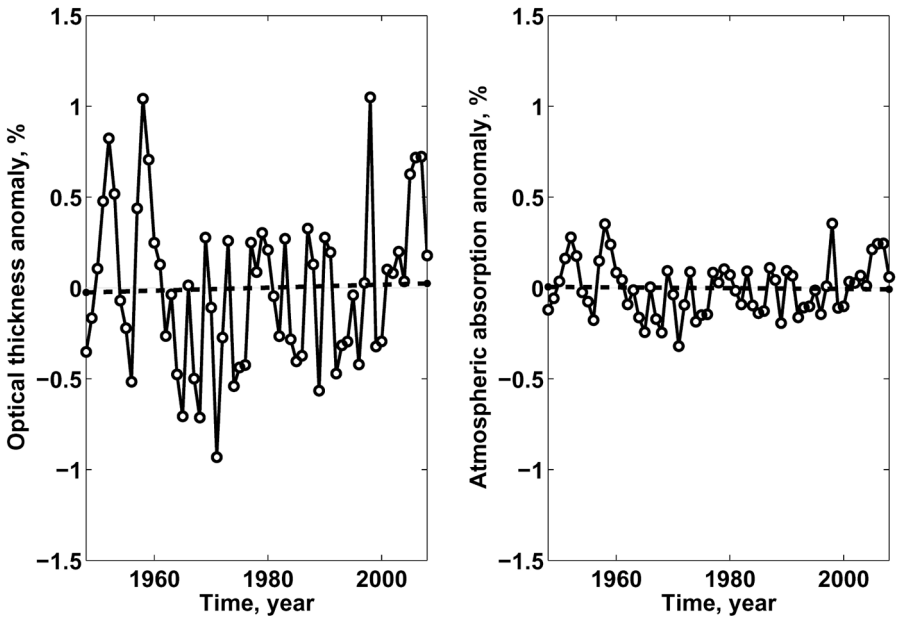

Figure 10. Time dependence of τ_A and A in the NOAA NCEP/NCAR annual global mean reanalysis time series. The thick dashed lines are the linear trend lines. The reference values (61 year means) of τ_A and A are 1.868754 and 0.84568, respectively.

One may already conclude that using the more conservative $\Delta\tau_A = 0.00179$ value for about 21 % increase in CO_2, and assuming that the atmosphere would behave similarly for CO_2 doubling, the predicted change in τ_A is $\Delta\tau_A = 100\times0.00179/21.63 = 0.00827$. This is one third of the no-feedback change of $\Delta\tau_A = 0.0246$ for CO_2 doubling. In other word, GCMs or other climate models, using a no-feedback optical thickness change for their initial CO_2 sensitivity estimates, they already start with a minimum of 200 % error (overestimate) just in $\Delta\tau_A$.

4 Virtual Primary No-Feedback Effect

For comparison with the empirical observations above, we also compute theoretically a virtual reference signal, the primary no-feedback effect of the actually measured increase in atmospheric CO_2 over the 61 years. The virtual effect is the difference between the actual signal and the computed virtual reference signal. The virtual effect is not stochastically affected by the year-to-year fluctuations, because it is a virtual change, defined conceptually and mathematically, not empirically.

Fortunately here we are dealing with very small changes and the optical thickness response of the system for the perturbations may reasonably be assumed to be linear, that is to say, the incremental response is directly proportional to the incremental perturbation. The minimum and maximum optical thicknesses are 1.8513 and 1.8884 respectively. The optical thickness of the average profile is $\tau_A(\overline{c},\overline{u},\overline{t_A}) = 1.86877$, and the average of 61 optical thicknesses is $\overline{\tau_A(c,u,t_A)} = 1.86875$. The bar over the variable vectors now indicates averaging over the 61 years. The effect of changes in c, u, and t_A may be computed by two different ways. One way is to compare the actual $\tau_A(c,u,t_A)$ to the ones where one variable is kept at the average value, and the other way is to compare the average $\tau_A(\overline{c},\overline{u},\overline{t_A})$ to the ones where one variable vector is replaced with the actual one. These two methods are termed as dual or single profile perturbations, and they result in the same changes in τ_A. We may write:

$$\Delta\tau(c) = \tau_A(c,u,t_A) - \tau_A(\overline{c},u,t_A) = \tau_A(c,\overline{u},\overline{t_A}) - \tau_A(\overline{c},\overline{u},\overline{t_A}), \tag{13a}$$

$$\Delta\tau(u) = \tau_A(c,u,t_A) - \tau_A(c,\overline{u},t_A) = \tau_A(\overline{c},u,\overline{t_A}) - \tau_A(\overline{c},\overline{u},\overline{t_A}), \tag{13b}$$

$$\Delta\tau(t_A) = \tau_A(c,u,t_A) - \tau_A(c,u,\overline{t_A}) = \tau_A(\overline{c},\overline{u},t_A) - \tau_A(\overline{c},\overline{u},\overline{t_A}). \tag{13c}$$

In Fig. 11 we present the annual variations in $\Delta\tau(c)$, $\Delta\tau(u)$ and $\Delta\tau(t_A)$. As it was expected the cumulative changes in τ_A are simply the arithmetic sum of the changes due to the individual variables. Clearly, the variation in the annual mean optical thickness anomaly is largely caused by the H_2O, $\Delta\tau \cong \Delta\tau(u)$, the linear correlation coefficient between $\Delta\tau(u)$ and $\Delta\tau$ is 0.9948. The $\Delta\tau(c)$ and $\Delta\tau(t_A)$ works into the opposite direction and neither of them has significant correlation with the $\Delta\tau$. The numerical values are 0.131 for CO_2, and –0.494 for the temperature.

As a final conclusion of this perturbation study, we can safely state that the dynamic stability of the stationary value of the true greenhouse-gas optical thickness of the atmosphere is mediated mainly by the amount and distribution of the water vapor in the atmosphere, and by the surface and atmospheric temperatures. For a recent reference, applying eqn (6) and the Earth's long wave global average surface radiation budget data (from Table 1b in Ref. 19), the global average all-sky true optical thickness is 1.8779. This value was computed as the average from four independent groups. Radiation budget data from Ref. 16 were not included. Apparently, the global average cloud cover must not have a dramatic effect on the global average clear-sky optical thickness, and the effective altitude of the global average cloud cover must be around 2 km, as it was theoretically predicted in [4].

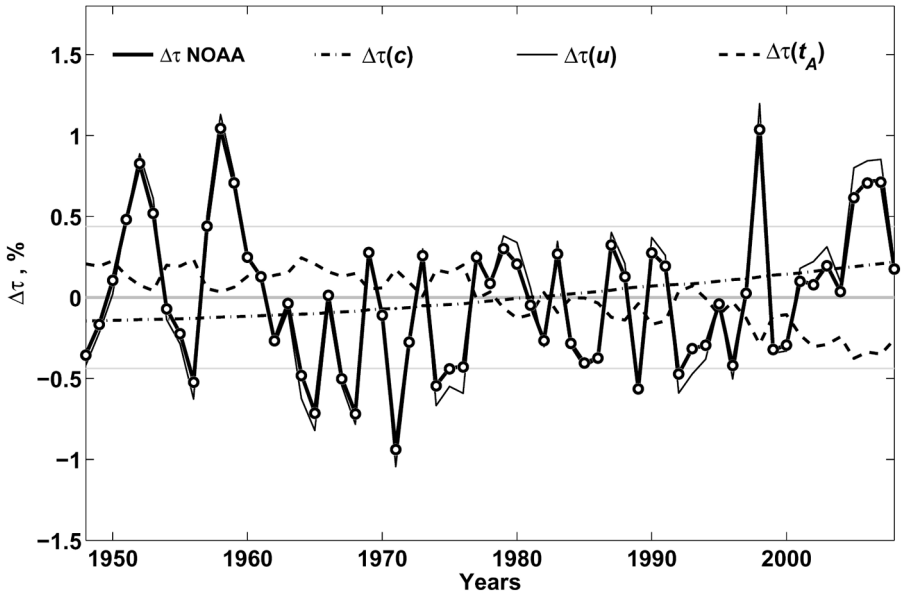

Figure 11. Summary of the perturbation study with the NOAA annual mean time series data. Here the normalized variability is plotted for the CO_2, H_2O and temperature perturbations. The reference value (61 year mean) of τ_A is 1.868754. The open circles indicate the sum of the $\Delta\tau(c)$, $\Delta\tau(u)$, and $\Delta\tau(t_A)$ curves. The thick black $\Delta\tau$ curve is the unperturbed anomaly in the original τ_A. Obviously, the fluctuations of global average $\Delta\tau$ are very largely explained immediately and directly by variations in water vapor column amounts.

5 Statistical Testing

The linear regression coefficient of the actual values of τ_A against time has a Student *t* value of 0.499. This is not even nearly statistically significantly different from zero. The Student *t* value that would correspond to the theoretically calculated virtual effect of actual CO_2 is 1.940. This would be statistically significant on a one-sided test at the 0.05 significance level. The statistical power of the Student *t* test for these data at a one-sided significance level of 0.05 is 0.6. That is to say, the data are well enough behaved to detect at the one-sided significance level 0.05, with a probability of 0.6, an uncompensated effect of CO_2 of the magnitude of the theoretically calculated virtual effect, supposing the same degree of variability in the data, if it were present in them. For putative data with this degree of scatter, there is a probability of 0.4 that such an effect, though putatively present, would not be considered statistically significant at the one-sided significance level of 0.05.

CONCLUSIONS

The greenhouse effect is here monitored without the superfluous complications of AOGCM climate models. The present method shows directly whether the global average infrared absorption properties of the atmosphere are changing or not. In general, if there has been global warming due to any cause, its possible correlation with

infrared absorption properties of the atmosphere will be directly apparent from accurate observations assessed by calculations of the absorption properties. The present results show an apparent warming associated with no apparent change in the absorption properties. Change in absorption properties cannot have been the cause of the warming.

The results show that the theoretical CO_2-induced virtual increase in true greenhouse-gas optical thickness greatly exceeds the actual empirically measured change over the 61-year dataset. The fact that the virtual change is about four times the actual change is strong empirical evidence that there is a very strong dynamic compensation that stabilizes the atmospheric energy transport process against a potential perturbation by CO_2 change. This means that the empirically estimated virtual feedback of water vapor effect on the greenhouse-gas optical thickness is not significantly positive contradicting the IPCC doctrine of it being strongly positive. It is clear from these data that the increase in surface temperature shown in Fig. 9 cannot in the least be accounted for by any effect of CO_2 on greenhouse gas optical thickness, with or without positive feedback by water vapor. Merely empirical evidence does not necessarily justify predictions of the future: for them, in addition to empirical evidence, some logical warrant of generality is needed. Such a warrant of generality is usually called a physical theory. In order to predict the future, we need a principled physical theory to explain our empirical observations. The present paper has restricted its attention to the empirical observational testing of the quasi-all-sky model, and has avoided theoretical analysis. These empirical results could well be challenged by a comparable empirical method.

ACKNOWLEDGEMENT

I am very grateful for the valuable discussions with Christopher Game and Jan Pompe and for their invaluable help in the preparation of the manuscript. The interest and help obtained from the Lavoisier Group is much appreciated. Also, I wish to thank K. Gregory, (Friends of Science Society), D. Stockwell, D. Hagen, S. Welcenbach and A. Harvey for their support and encouragement obtained in the early stages of this investigation. Also I wish to thank for the careful work of the three Referees.

REFERENCES

1. Hansen, J., Johnson, D., Lacis, A., Lebedeff, S., Lee, P., Rind, D., Russell, G., Climate impact of increasing atmospheric carbon dioxide, *Science*, 1981 , 213, 957–966.
2. Ramanathan, V., 1981, The role of ocean-atmosphere interactions in the CO_2 climate problem, *Journal of the Atmospheric Sciences*, 1981, 38, 918–930.
3. Bony, S., Colman, R., Kattisov, V.M., Allan, R.P., Bretherton, C.S., Dufresne, J.-L., Hall,A., Hallegatte,S., Holland, M.M., Ingram, W., Randall, D.A., Soden, B.J., Tselioudis, G., Webb,M.J., How well do we understand and evaluate climate change feedback processes?, *Journal of Climate*, 2006, 19: 3445–3482.
4. Miskolczi, F.M., Greenhouse effect in Semi-transparent Planetary Atmospheres, *Quarterly Journal of the Hungarian Meteorological Service*, 2007, 111(1), 1–40.
5. Collins, G.W. II., *The Fundamentals of Stellar Astrophysics. Part II. Stellar Atmospheres*. WEB edition, 2003:

6. Mihalas, D. and Weibel-Mihalas, B., *Foundations of Radiation Hydrodynamics*, Dover Publications, Inc. Mineola, NY, 1999

7. Miskolczi, F.M., *High Resolution Armospheric Radiative Transfer Code (HARTCODE)* Technical Report, IMGA-CNR, Modena, Italy, 1989

8. Miskolczi, F.M. and Guzzi, R., Effect of Non-uniform Spectral Dome Transmittance on the Accuracy of Infrared Radiation Measurements Using Shielded Pyrradiometers and Pyrgeometers, *Applied Optics*, 1993, 32(9), 3257–3265

9. Miskolczi, F., Modeling of Downward Surface Flux Density for Global Change Applications and Comparison with Pyrgeometer Measurements, *Journal of Atmospheric and Oceanic Technology*, 1994, 11(2), 608–612

10. Miskolczi, F.M., High Accuracy Skin Temperature Retrieval from Spectral Data of Multichannel IR Imagers, *Quarterly Journal of the Hungarian Meteorological Service*, 2001, 105(4)-106(1), 243–251

11. Miskolczi, F.M. and Mlynczak, M.G., The Greenhouse Effect and the Spectral Decomposition of the Clear-Sky Terrestrial Radiation, *Quarterly Journal of the Hungarian Meteorological Service*, 2004, 108(4) 209–251

12. Kratz, D.P., Mlynczak, M.G., Mertens, C.J., Brindley, H., Gordley, L.L., Martin-Torres, J., Miskolczi, F.M., Turner, D.D., An Inter-Comparison of Far-Infrared Line-by-Line Radiative Transfer Models, *Journal of Quantitative Spectroscopy and Radiative Transfer*, 2005, 90, 323–341

13. Chedin, A. and Scott, N.A., *The Improved Initialization Inversion Procedure (3I)*, 1983:.Laboratoire de meteorologie dynamique, Centre National de la Recherche Scientifique, Note Interne LMD, No. 117

14. NOAA NCEP/NCAR Reanalysis data time series, http://www.cdc.noaa.gov,2008

15. ERBE Monthly Scanner Data Product. NASA Langley Research Center, Langley DAAC User and Data Services, 2004, userserv@eosdis.larc.nasa.gov

16. Kiehl, J.T. and Trenberth, K.E., Earth's Annual Global Mean Energy Budget, *Bulletin of the American Meteorological Society*, 1997, 78(2), 197–208

17. Prevost, P., Mémoire sur l'équilibre du feu, *Journal de Physique*, 1791, 30, 314–323.

18. Paltridge, G., Arking, A., Pook, M., Trends in Middle- and Upper-level Tropospheric Humidity from NCEP Reanalysis Data, *Theoretical Applied Climatology*, 2009 DOI: 10.1007/s00704-009-0117-x

19. Trenberth, K. E., Fasullo, J.T. and Kiehl, J., 2009: Earth's Global Mean Energy Budget, *Bulletin of the American Meteorological Society*, 2009, March, 311-323